AIMS Materials Science, 9(4): 617–627.
DOI: 10.3934/matersci.2022037
Received: 12 May 2022
Revised: 06 July 2022
Accepted: 17 July 2022
Published: 8 August 2022

http://www.aimspress.com/journal/Materials

Research article

Understanding the structural properties of feasible chemically reduced graphene

Nur Ezyanie Safie and Mohd Asyadi Azam*

Fakulti Kejuruteraan Pembuatan, Universiti Teknikal Malaysia Melaka, Hang Tuah Jaya, 76100 Durian Tunggal, Melaka, Malaysia

* **Correspondence:** Email: asyadi@utem.edu.my; Tel: +6012-5048957.

Abstract: The production of pristine graphene materials for industrialization, often limited by the complicated synthesis route, has introduced other graphene derivatives with a workable and facile synthesis route, especially for mass production. For the chemical exfoliation process, the synthesis involves oxidants and reducing agents to exfoliate the graphene layer from the 3D graphite and remove excess oxygen-containing functional groups yielding graphene-like materials known as reduced graphene oxide (rGO). This work feasibly produces rGO with nanoplatelet morphology through the green solution-processable method. Upon reduction, the crystallite size for the a-axis (L_a) is more prominent (22.50 Å) than the crystallite size for the c-axis (L_c) (11.50 Å), suggesting the nanoplatelets structure of the end product, which is also confirmed by the morphology. The integrated intensity (I_D/I_G) ratio and average defect density (n_D) of as-prepared rGO confirmed the sp^2 restoration in the graphitic structure. Overall, the Raman and X-ray diffraction (XRD) characterization parameters validate the production of rGO nanoplatelets, especially with four graphene layers per domain, suggesting that high-quality rGO are achievable and ready to be implemented for the large-scale production.

Keywords: reduced graphene oxide; exfoliated graphene; feasible method; green route production; structural properties

1. Introduction

Graphene, a single-layered carbon arranged in a honeycomb structure, has attracted massive scientific interest due to its fascinating electronic, mechanical, and thermal properties, especially in photovoltaic applications [1–3]. However, since pristine graphene generally has zero band gaps [4], the application of graphene is limited in thin-film solar cells such as perovskite solar cells leads to the introduction of graphene derivatives such as graphene oxide (GO) and reduced graphene oxide (rGO) [5]. The bandgap of graphene derivatives is tunable depending on the surface functionalization [6,7], making it favorable materials to be incorporated into the photovoltaic devices where the matching energy levels of the materials used in each component contribute to the efficiency of device performance. Besides, rGO is designated as a decent option to that pristine graphene as it can restore the good mechanical [8,9] and optoelectronic [10,11] properties as reported in the literature. The defect in the rGO structure due to the removal of a few oxygen-containing functional groups during its synthesis process distinguishes it from the pristine graphene. Also, the remaining oxygen-containing functional group in the rGO structure opens up to the surface engineering of the composite reinforcement for broad applications, including energy storage [12,13], building material [14], sensor [15], anti-corrosion material [16] and photovoltaic [17].

Generally, the graphene synthesis route starts either from the top-down or bottom-up method where the starting material differs, which are graphite and carbon gas sources, respectively. Usually, high conductivity graphene sheet is produced from the bottom-up method. However, the high cost and complex procedure set up limits the utilization. The top-down method offers a low-cost procedure with a high-quality end product via mechanical exfoliation [18] and a high-productivity end product via liquid-phase exfoliation [19]. In terms of solution-processable solar cells application, high-dispersity graphene derivative is favoured to be integrated into the device architecture. Thus, the liquid phase exfoliation method attracted attention in this field.

Nonetheless, one of the critical challenges in synthesizing bulk-quantity graphene sheets via the top-down method in industrial is overcoming the intense, cohesive Van Der Waals' energy of the p-stacked layers in graphite. However, large amounts of graphene derivatives are quickly produced via the oxidation process of graphite [20]. To date, the chemical reduction of GO has become the most widely used method for preparing graphene derivatives due to its cost-effectiveness and bulk productivity. However, this method usually involves highly toxic chemicals, such as hydrazine [21], hydroquinone [22], and sodium borohydride [23], which harm human health and the environment.

Therefore, it is highly desired to develop and introduce less-or non-toxic reducing agents to replace these harmful chemicals, especially concerning the mass production of high-quality rGO. From the works of literature, few numbers of non-toxic reducing agents are introduced, including proteins [24], plant extracts [25], and organic compounds [26]. Since non-toxic reducing agents promote an inexpensive and green environment for the reduction process, it is desirable to develop sustainable technologies to produce graphene derivatives to cater the industrial needs. Ascorbic acid is one of the remarkable non-toxic reducing agents because the rGO quality is comparable to hydrazine. Furthermore, rGO formed by reduction using ascorbic acid showed better restoration of aromatic structure than hydrazine [27]. Thus, this work demonstrated the production of rGO by using ascorbic acid as the non-toxic reducing agent to produce rGO with high quality to facilitate the bulk production of graphene derivatives.

Usually, the GO was formed from the top-down method and then reduced by the reducing agents. This work highlights the expedited route to synthesizing rGO straight from the graphite oxide suspension without undergoing GO formation. The one-pot stir-sonicate technique can expedite the rGO synthesis route and efficiently reduce using non-toxic ascorbic acid. The fully solution-processable synthesis method started with the oxidation phase to cut the sizeable sp^2 carbon sheets into nanosheets following the modified Hummer's method. Then, exfoliation occurs during the stirring-sonication method, followed by the reduction process where the restoring of sp^2 graphitic structure happens through removing a few oxygen-containing functional groups. This work aims to contribute to the knowledge of a facile way of characterizing the quality of high-productivity rGO nanoplatelets in terms of structural properties via Raman and X-ray diffraction (XRD) parameters that discuss defects in the graphene regions. Also, the high-quality rGO with nanoplatelets-shaped validated by three different spots of the FESEM images.

2. Materials and method

2.1. Synthesis of GO

GO was synthesized from graphite via a modified Hummer's method [28] in this work. Briefly, 1 g graphite fine powder (≥ 99.5%, Merck) was stirred in an ice-water bath with the addition of 50 mL H_2SO_4 (95%, Sigma Aldrich) until the temperature was reduced below 10 ℃. 3 g of $KMnO_4$ (99%, R&M Chemical) was gradually added before alternately stirring the suspension at room temperature for 25 min, followed by 5 min sonication in an ultrasonic bath. The stirring-sonication step was repeated alternately for 6 h. Then, 200 mL of distilled water was slowly added to quench the reaction and continued with sonication for 2 h to produce a graphite oxide solution that was later will divided into two equal parts (one part was further processed for preparation rGO as described below). One part is used for GO synthesis for comparison purposes. Next, for the GO exfoliation process, 20 mL of H_2O_2 (30%, Sigma Aldrich) was added gradually into the graphite oxide solution until gas evolution ceased. The suspension was washed with 1M HCl (37%, R&M Chemical) acid solution and distilled water several times until reaching pH 7 and filtered to get the precipitate. The final precipitates were dried in the oven at 60 ℃ for 24 h and well ground to get GO powder.

2.2. Reduction of GO

For the reduction, ascorbic acid was used as the reducing agent [29]. The rGO production can be expedited from the graphite oxide suspension in this work. First, 1M NaOH (R&M Chemical) solution was added to the exfoliated graphite oxide solution until reaching pH 6. Then, the suspension was sonicated for 1 h before slowly adding 0.1 g/mL of dilute ascorbic acid at room temperature before increasing the temperature to 95 ℃, where the reduction takes place for 1 h. The resultant black precipitates were filtered and washed with a 1M HCl acid solution and deionized water to neutral pH. Finally, the filtrate was dried in the oven at 60 ℃ overnight and further ground to get rGO powder as the final product. This work yielded 1.4 g of rGO powder by 1 g of starting material, graphite.

2.3. Instrumentation

For structural characterization, the XRD measurement of rGO powder was gained by X-ray diffractometer (PANalytical, X'PERT PRO) instrument with the Cu K α (1.5418 Å) radiation excitation source. Raman analysis was performed to confirm further the rGO phase and structure using a UniRAM-3500 Raman spectrometer equipped with the incident laser light of 532 nm. The morphology and energy-dispersive X-ray (EDX) spectroscopy elemental mapping of the rGO powder was observed by Hitachi-SU8000 field emission scanning microscopy (FESEM) with an operating voltage of 5.0 kV.

3. Results and discussion

3.1. Structural and morphology characterization

Raman measurement carries essential information about the crystal structure of graphene derivatives and the possible presence of disorder or defects in graphitic structure mainly caused by the synthesis route of the material. The Raman spectrum in Figure 1 shows two dominant bands for graphene derivatives in which their position and shape provide information on their properties. The G band is the primary mode representing the planar configuration of sp^2 bonded carbons in graphene-based materials. Pristine graphite shows a sharp G peak, centred at 1558 cm^{-1} because of the first-order scattering of E_2g mode [30], while for GO and rGO, these peaks are centred at 1572 and 1571 cm^{-1}, respectively. On the other hand, the D band represents the 'disorder band' or the 'defect band' that shows defects caused by breaking in the infinite's symmetry carbon honeycomb-shaped lattice. The peak is centred at 1340, 1352, and 1347 cm^{-1} for graphite, GO, and rGO. After the conversion of graphite to GO, the D and G peaks broaden and rise in their intensity because of the introduction of oxygen-containing functional groups into the graphitic planes. Besides, the G band also widens and shifts to a higher wavenumber, which is from 1558 to 1572 cm^{-1}. The change in position of the G band to a higher wavenumber upon the oxidation of graphite indicates amorphization of the graphite with a substantial fraction of sp^3 carbon. However, the G peak in rGO shifted to the lower wavenumber, which identifies the removal of a few oxygen-containing functional groups [31].

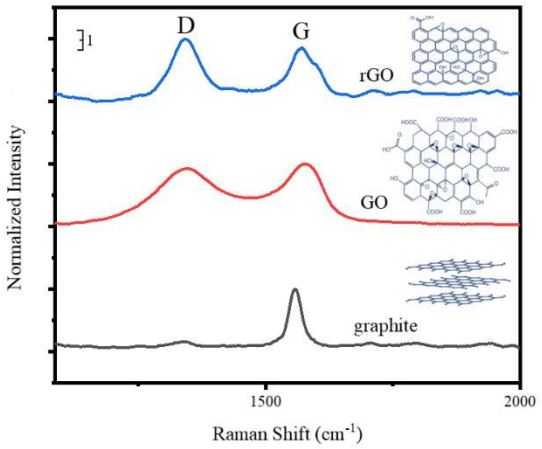

Figure 1. Raman spectra of the graphite, GO, and rGO (insert is the chemical structure of graphite, GO, and rGO).

The integrated intensity (I_D/I_G) ratio characterizes the disorder of the graphitic structure. The I_D/I_G value of graphite, GO, and rGO were found to be 0.19, 0.64, and 1.33, respectively, in this work. GO obtained a higher I_D/I_G ratio than pristine graphite, which confirms the oxidation of pristine graphite occurred, making the D band appear caused by the hybridization of graphitic order. The presence of an oxygen functional group in the GO structure would lead to a defect in the graphitic structure. Thus, there would be more sp^3 carbon atoms corresponding to the defects in the GO structure. After the chemical reduction of GO to rGO, the I_D/I_G ratio obtained also increased compared to GO.

In contrast, the increment of the I_D/I_G ratio is not because of the defect in the structure. Since GO does not comprise a purely sp^2 structure but a highly disordered structure with a significant sp^3 content, the decrease of defects in GO structure after reduction would increase the I_D/I_G ratio. After the reduction process, more sp^2 carbon atoms surround the defect structure to show a considerable recovery of the conjugated graphitic framework upon vanishing oxygen-containing functional groups during the exfoliation process. The restoring of sp^2 carbon domains happened in the rGO structure, which can be proven by the high weight percentage, wt% of the carbon element in the rGO structure obtained from EDX analysis. The average defect density, (n_D) presence in the graphitic ordering of the graphene-based materials can be calculated based on Eq 1 [32,33]:

$$\eta_D = \frac{(1.85 \pm 0.5) \times 10^{22}}{\lambda_{laser}^4} \left(\frac{I_D}{I_G} \right) \tag{1}$$

Where λ_{laser} is the wavelength of the Raman laser source (532 nm for this work). The calculated value of n_D can be summarized according to the order of rGO > GO > graphite (Table 1). Both GO, and rGO obtained a higher calculated value of n_D than pristine graphite because of the excessive hybridization of its graphitic lattice throughout the synthesis route. The Raman peak positions, I_D/I_G ratios, and defect density of graphite, GO, and rGO are summarized in Table 1.

Table 1. Peak position of the D and G bands, I_D/I_G ratio, and defect density of the graphite, graphene oxide (GO), and reduced graphene oxide (rGO).

Materials	Peak position (cm^{-1})		Calculated Integrated intensity		I_D/I_G ratio	Defect density, n_D (cm^{-2}) ($\times 10^{11}$)
	D band	G band	D band	G band		
Graphite	1340	1558	6311.50	33926.24	0.19	0.32–0.56
GO	1352	1572	294879.05	461638.57	0.64	1.08–1.88
rGO	1347	1568	61386.20	46237.41	1.33	2.24–3.90

The XRD pattern shown in Figure 2 depicted a prominent diffraction peak of (002) plane centred at a 2θ value of 24.42°, indicating average inter-planar spacing, d_{002} of 3.64 Å for the as-prepared rGO nanoplatelets. This value has been calculated using the Bragg's equation (Eq 2):

$$d_{002} = \frac{n\lambda}{2\sin\theta} \tag{2}$$

Where d_{002} is the inter-planar spacing, λ is the wavelength of the x-ray source (in this work, the value is 1.5418 Å referring to the Cu laser), and θ is half of the correlated diffraction angle of the (002) plane. The value obtained is higher when compared to the reported pristine graphite in literature, which is d~3.4 Å [34].

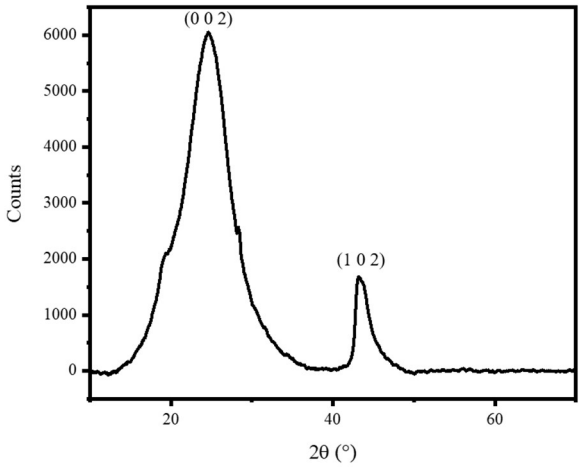

Figure 2. XRD pattern of as-prepared rGO.

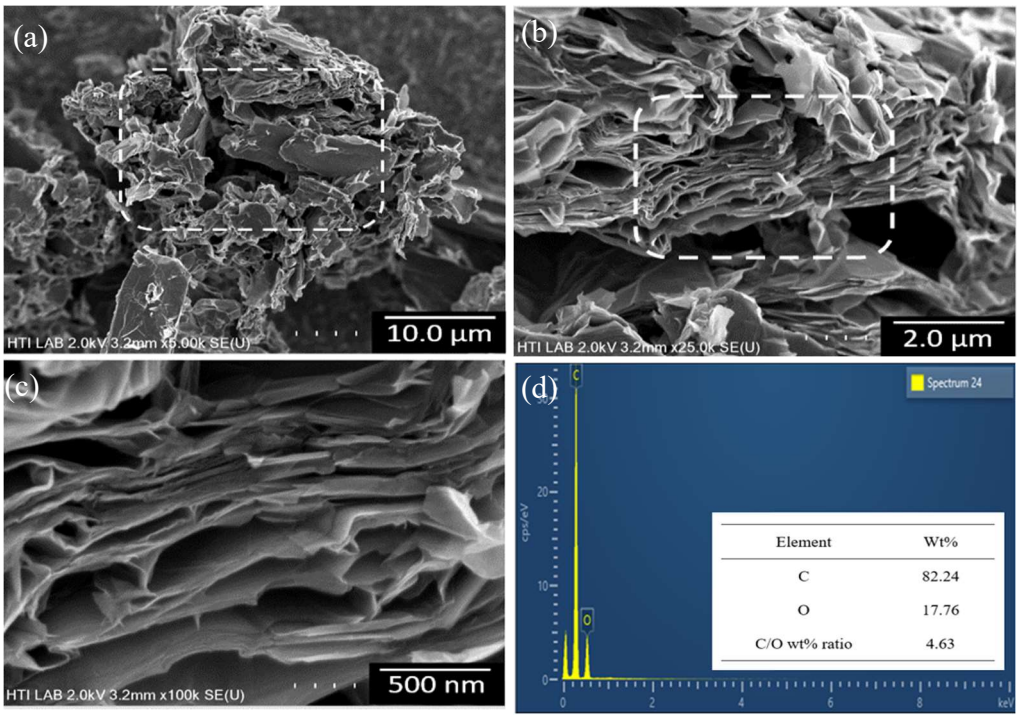

Figure 3. FESEM image (spot 1) and EDX pattern of as-prepared rGO.

The increment of the inter-planar spacing of rGO compared to graphite suggested the presence of few remaining oxygen-containing groups on the as-prepared rGO nanoplatelets. The first spot of the FESEM image in Figure 3 depicted inter-planar spacing in the rGO structure and suggested well-exfoliated rGO nanoplatelets as the final product. The insertion of oxygen happens through the oxidation process of graphite to assist in the formation of the exfoliated graphite oxide layer. This process has happened before the reduction process takes place to produce rGO. Also, a small diffraction peak appears at 2θ of 43.68°, corresponding to the (102) plane conforming to the rGO structure [35].

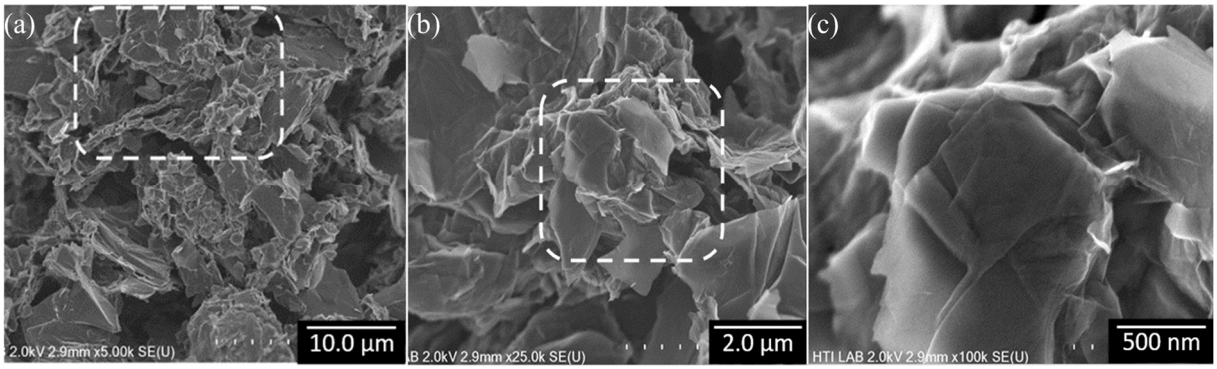

Figure 4. FESEM image of as-prepared rGO nanoplatelets (spot 2).

Besides, the XRD spectrum also shows a broader and less intense peak than graphite reported from literature [36,37], which validates the stacking of randomly packed rGO nanoplatelets, which can be seen from the FESEM image in Figure 4. Besides, the peaks' width of the XRD spectrum gives insight into the graphitic domains' presence in the macroscopic graphene sheets and is responsible for evaluating the average size of the sp^2 cluster in graphene-based materials [38]. The average crystallite size along the c-axis (L_c) and a-axis (L_a) can be calculated from the well-known Debye-Scherrer equation as follows Eq 3:

$$L = \frac{k\lambda}{\beta \cos\theta} \tag{3}$$

Where k is the shape factor (L_c~0.94; L_a~1.84) [39], λ is the wavelength of the x-ray source, β is the full width at half-maximum (FWHM) of the diffraction peak, and θ is half of the correlated diffraction angle (2θ~24.42° for L_c; 2θ~43.68° for L_a). The obtained calculated L_a is larger (22.50 Å) than L_c (11.50 Å) for the as-prepared rGO showing the domain size is more prominent in the in-plan graphitic ordering manner and observable in the second spot of the FESEM image in Figure 4. Aside from the well exfoliated as-prepared rGO nanoplatelets, the common feature of crumpled and aggregated rGO nanoplatelets is pictured in the FESEM image, which is dependent on the chemical exfoliation methods in the synthesis route [40].

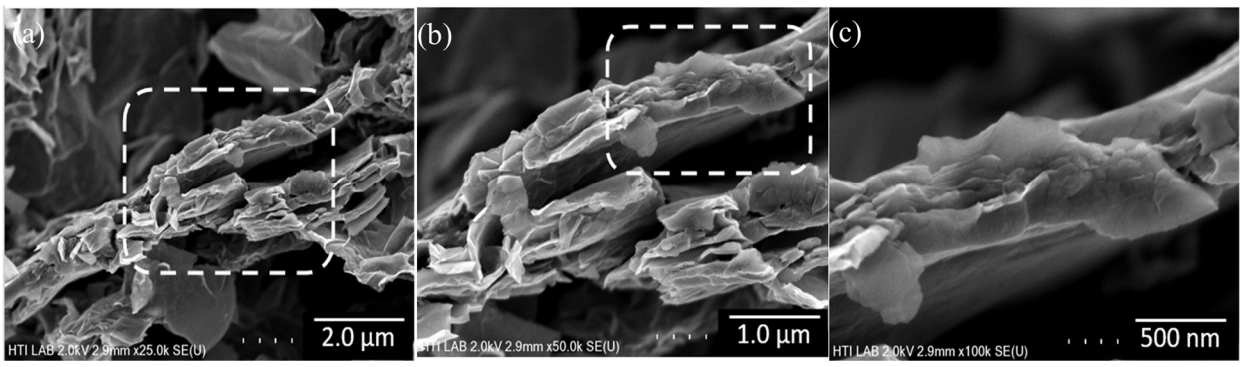

Figure 5. FESEM image of as-prepared rGO nanoplatelets (spot 3).

Meanwhile, the average number of graphene layers (n) per domain can be calculated from the

XRD pattern using the combination of Bragg's equation (Eq 1) and Debye-Scherer Eq 2, which gives expression as follows Eq 4 [38]:

$$\eta = \left(\frac{L_c}{d} + 1 \right) \tag{4}$$

From the calculation, as-prepared rGO is reported to have an average of 4 graphene layers per domain, which is also pictured under a third spot of the FESEM image in Figure 5. The presence of fewer graphene layers is essential for rGO production to ensure the efficient reduction process as eliminating a few oxygen-containing functional groups dissipating the inter-layer attraction and surface contact, hence expected to improve the electrical conductivity [41] and reduce the hydrophilicity [42] of the rGO as compared to GO. Overall, the defect present in the rGO structure because of the synthesis procedure would be beneficial for further hybridization with a photoactive molecule, polymer, and nanoparticle to create a composite system which is remarkably beneficial for various applications, including photovoltaic and optoelectronic devices. Table 2 summarizes the physical parameters calculated from the XRD analysis, confirming the high quality of rGO nanoplatelets prepared in this work.

Table 2. Physical parameters obtained from XRD analysis of reduced graphene oxide (rGO).

Materials	2θ° of (002) plane	Inter-planar spacing, d_{002} (Å)	Crystallite size along c-axis, L_c (Å)	Crystallite size along a-axis, L_a (Å)	Number of layers per domain, n
rGO	24.42	3.64	11.50	87.45	4

4. Conclusion

In summary, the facile and green synthesis route demonstrated in this work successfully yielded the high productivity of rGO nanoplatelets. Raman and XRD analysis confirm the hybridization of graphitic ordering from the starting material, graphite, to the final products, rGO nanoplatelets. The I_D/I_G ratio value from GO to rGO shows victorious restoring of the sp^2 domain upon the reduction process using ascorbic acid as the environmental-friendly reducing agent. The nanoplatelet structure of rGO was also validated by the physical parameters calculated from the XRD analysis and the three different spots of the FESEM images. An average of four graphene layers per domain successfully achieved in this work suggested that this green production approach can expedite the mass production in industrialization and yield high productivity and quality of rGO nanoplatelets for further use in broad as optoelectronic, photovoltaic, and environmental applications.

Acknowledgments

The authors are grateful to Universiti Teknikal Malaysia Melaka for the facilities support and the UTeM Zamalah Scheme for PhD support of NE Safie.

Conflict of Interest

The authors declare have no interests in this paper.

References

1. O'keeffe P, Catone D, Paladini A, et al. (2019) Graphene-Induced improvements of perovskite solar cell stability: effects on hot-carriers. *Nano Lett* 19: 684–691. https://doi.org/10.1021/acs.nanolett.8b03685.
2. Biccari F, Gabelloni F, Burzi E, et al. (2017) Graphene-based electron transport layers in perovskite solar cells: a step-up for an efficient carrier collectio. *Adv Energy Mater* 7: 1701349. https://doi.org/10.1002/aenm.201701349
3. Azam MA, Aziz MFA, Zulkapli NN, et al. (2020) Direct observation of graphene during Raman analysis and the effect of precursor solution parameter on the graphene structures. *Diam Relat Mater* 104: 107767. https://doi.org/10.1016/j.diamond.2020.107767.
4. Das S, Pandey D, Thomas J, et al. (2019) The Role of graphene and other 2D Materials in solar photovoltaics. *Adv Mater* 31: 1–35. https://doi.org/10.1002/adma.201802722.
5. Safie NE, Azam MA, Aziz MFA, et al. (2021) Recent progress of graphene-based materials for efficient charge transfer and device performance stability in perovskite solar cells. *Int J Energy Res* 45: 1347–1374. https://doi.org/10.1002/er.5876.
6. Ramar V, Balasubramanian K (2018) Charge transfer induced tunable bandgap and enhanced saturable absorption behavior in rGO/WO_3 composites. *Appl Phys A* 124: 1–11. https://doi.org/10.1007/s00339-018-2191-3.
7. Méndez-Romero UA, Pérez-García SA, Xu X, et al. (2019) Functionalized reduced graphene oxide with tunable band gap and good solubility in organic solvents. *Carbon* 146: 491–502. https://doi.org/10.1016/j.carbon.2019.02.023.
8. Wang T, Zhao R, Zhan K, et al. (2020) Preparation of electro-reduced graphene oxide/copper composite foils with simultaneously enhanced thermal and mechanical properties by DC electro-deposition method. *Mater Sci Eng A* 805: 140574. https://doi.org/10.1016/j.msea.2020.140574.
9. Liang W, Zhang G (2020) Effect of reduced graphene oxide on the early-age mechanical properties of geopolymer cement. *Mater Lett* 276: 128223. https://doi.org/10.1016/j.matlet.2020.128223.
10. Kumar H, Sharma R, Yadav A, et al. (2020) Synthesis, characterization and influence of reduced Graphene Oxide (rGO) on the performance of mixed metal oxide nano-composite as optoelectronic material and corrosion inhibitor. *Chem Data Collect* 29: 100527. https://doi.org/10.1016/j.cdc.2020.100527.
11. Yang HY, Lee HJ, Jun Y, et al. (2020) Broadband photoresponse of flexible textured reduced graphene oxide films. *Thin Solid Films* 697: 137785. https://doi.org/10.1016/j.tsf.2020.137785.
12. Vidhya MS, Ravi G, Yuvakkumar R, et al. (2020) Functional reduced graphene oxide/cobalt hydroxide composite for energy storage applications. *Mater Lett* 276: 128193. https://doi.org/10.1016/j.matlet.2020.128193.
13. Galal A, Hassan HK, Atta NF, et al. (2018) Effect of redox electrolyte on the specific capacitance of $SrRuO_3$-Reduced graphene oxide nanocomposites. *J Phys Chem C* 122: 11641–11650. https://doi.org/10.1021/acs.jpcc.8b02068.
14. Guo S, Lu Y, Wan X, et al. (2020) Preparation, characterization of highly dispersed reduced graphene oxide/epoxy resin and its application in alkali-activated slag composites. *Cem Concr Compos* 105: 10324. https://doi.org/10.1016/j.cemconcomp.2019.103424.

15. Gao W, Chen H, Cao J, et al. (2018) Size effect on the high-strength and electrically conductive polyolefin/reduced graphene oxide (RGO) composites. *J Phys Chem C* 122: 7968–7974. https://doi.org/10.1021/acs.jpcc.7b12787.
16. Kamil MP, Kim MJ, Ko YG (2020) Direct electro-co-deposition of Ni-reduced graphene oxide composite coating for anti-corrosion application. *Mater Lett* 273: 1–4. https://doi.org/10.1016/j.matlet.2020.127911.
17. Sarkar A, Rahaman A, Chakraborty K, et al. (2020) Organic heterojunctions of phthalocyanine-reduced graphene oxide above percolation threshold for photovoltaic application. *Mater Chem Phys* 253: 123418. https://doi.org/10.1016/j.matchemphys.2020.123418.
18. Baqiya MA, Nugraheni AY, Islamiyah W, et al. (2020) Structural study on graphene-based particles prepared from old coconut shell by acid–assisted mechanical exfoliation. *Adv Powder Technol* 31: 2072–2078. https://doi.org/10.1016/j.apt.2020.02.039.
19. Güler Ö, Tekeli M, Taşkın M, et al. (2021) The production of graphene by direct liquid phase exfoliation of graphite at moderate sonication power by using low boiling liquid media: The effect of liquid media on yield and optimization. *Ceram Int* 47: 521–533. https://doi.org/10.1016/j.ceramint.2020.08.159.
20. Sieradzka M, Ślusarczyk C, Fryczkowski R, et al. (2020) Insight into the effect of graphite grain sizes on the morphology, structure and electrical properties of reduced graphene oxide. *J Mater Res Technol* 9: 7059–7067. https://doi.org/10.1016/j.jmrt.2020.05.026.
21. Ramesh P, Amalraj S, Arunachalam P, et al. (2021) Covalent intercalation of hydrazine derived graphene oxide as an efficient 2D material for supercapacitor application. *Synth Met* 272: 116656. https://doi.org/10.1016/j.synthmet.2020.116656.
22. Vallés-García C, Montero-Lanzuela E, Navalon S, et al. (2020) Tuning the active sites in reduced graphene oxide by hydroquinone functionalization for the aerobic oxidations of thiophenol and indane. *Mol Catal* 493: 111093. https://doi.org/10.1016/j.mcat.2020.111093.
23. Hu J, Kong G, Zhu Y, et al. (2020) Ultrafast room-temperature reduction of graphene oxide by sodium borohydride, sodium molybdate and hydrochloric acid. *Chinese Chem Lett* 32: 543–547. https://doi.org/10.1016/j.cclet.2020.03.045.
24. Luo Y, Kong FY, Li C, et al. (2016) One-pot preparation of reduced graphene oxide-carbon nanotube decorated with Au nanoparticles based on protein for non-enzymatic electrochemical sensing of glucose. *Sens Actuators B Chem* 234: 625–632. https://doi.org/10.1016/j.snb.2016.05.046.
25. Yang J, Xia X, He K, et al. (2021) Green synthesis of reduced graphene oxide (RGO) using the plant extract of Salvia spinosa and evaluation of photothermal effect on pancreatic cancer cells. *J Mol Struct* 1245: 131064. https://doi.org/10.1016/j.molstruc.2021.131064.
26. Satheesh K, Jayavel R (2013) Synthesis and electrochemical properties of reduced graphene oxide via chemical reduction using thiourea as a reducing agent. *Mater Lett* 113: 5–8. https://doi.org/10.1016/j.matlet.2013.09.044.
27. Miranda C, Ramírez A, Sachse A, et al. (2019) Sulfonated graphenes: Efficient solid acid catalyst for the glycerol valorization. *Appl Catal A Gen* 580: 167–177. https://doi.org/10.1016/j.apcata.2019.04.010.
28. Abdolhosseinzadeh S, Asgharzadeh H, Kim HS (2015) Fast and fully-scalable synthesis of reduced graphene oxide. *Sci Rep* 5: 10160. https://doi.org/10.1038/srep10160.

29. Sanati A, Raeissi K, Karimzadeh F (2020) A cost-effective and green-reduced graphene oxide/polyurethane foam electrode for electrochemical applications. *FlatChem* 20: 100162. https://doi.org/10.1016/j.flatc.2020.100162.
30. Gurzęda B, Buchwald T, Krawczyk P (2020) Thermal exfoliation of electrochemically synthesized graphite intercalation compound with perrhenic acid. *J Solid State Electrochem* 24: 1363–1370. https://doi.org/10.1007/s10008-020-04642-x.
31. Ismail Z (2019) Green reduction of graphene oxide by plant extracts: A short review. *Ceram Int* 45: 23857–23868. https://doi.org/10.1016/j.ceramint.2019.08.114.
32. Song N, Cui S, Jiao D, et al. (2017) Layered nanofibrillated cellulose hybrid films as flexible lateral heat spreaders: The effect of graphene defect. *Carbon* 115: 338–346. https://doi.org/10.1016/j.carbon.2017.01.017.
33. Bhaskaram DS, Govindaraj G (2018) Carrier transport in reduced graphene oxide probed using raman spectroscopy. *J Phys Chem C* 122: 10303–10308. https://doi.org/10.1021/acs.jpcc.8b01311.
34. Abdolmaleki A, Mohamadi Z, Ensafi AA, et al. (2018) Efficient and stable HER electrocatalyst using Pt-nanoparticles@poly (3, 4–ethylene dioxythiophene) modified sulfonated graphene nanocomposite. *Int J Hydrog Energy* 43: 8323–8332. https://doi.org/10.1016/j.ijhydene.2018.03.142.
35. Gupta B, Kumar N, Panda K, et al. (2017) Role of oxygen functional groups in reduced graphene oxide for lubrication. *Sci Rep* 7: 1–14. https://doi.org/10.1038/srep45030.
36. Morales-Acosta D, Flores-Oyervides JD, Rodríguez-González JA, et al. (2019) Comparative methods for reduction and sulfonation of graphene oxide for fuel cell electrode applications. *Int J Hydrog Energy* 44: 12356–12364. https://doi.org/10.1016/j.ijhydene.2019.02.091.
37. Dan L, Pope MA, Elias AL (2018) Solution-Processed conductive biocomposites based on polyhydroxybutyrate and reduced graphene oxide. *J Phys Chem C* 122: 17490–17500. https://doi.org/10.1021/acs.jpcc.8b02515.
38. Sharma R, Chadha N, Saini P (2017) Determination of defect density, crystallite size and number of graphene layers in graphene analogues using X-ray diffraction and Raman spectroscopy. *Indian J Pure Appl Phys* 55: 625–629.
39. Roy Chowdhury D, Singh C, Paul A (2014) Role of graphite precursor and sodium nitrate in graphite oxide synthesis. *RSC Adv* 4: 15138–15145. https://doi.org/10.1039/c4ra01019a.
40. Hou D, Liu Q, Cheng H, et al. (2017) Graphene synthesis via chemical reduction of graphene oxide using lemon extract. *J Nanosci Nanotechnol* 17: 6518–6523. https://doi.org/10.1166/jnn.2017.14426.
41. Burgos FJ, Llorente I (2019) Synthesis of Cu/rGO composites by chemical and thermal reduction of graphene oxide. *J Alloys Compd* 800: 379–391. https://doi.org/10.1016/j.jallcom.2019.06.008.
42. Kang Y, Obaid M, Jang J, et al. (2018) Novel sulfonated graphene oxide incorporated polysulfone nanocomposite membranes for enhanced-performance in ultrafiltration process. *Chemosphere* 207: 581–589. https://doi.org/10.1016/j.chemosphere.2018.05.141.

AIMS Press